Lattice Dynamics of β-V 2 O 5 : Raman Spectroscopic Insight into the Atomistic Structure of a High-Pressure Vanadium Pentoxide Polymorph

ARTICLE *in* INORGANIC CHEMISTRY · MARCH 2012

Impact Factor: 4.76 · DOI: 10.1021/ic202651b · Source: PubMed

8 AUTHORS, INCLUDING:

Rita Hadjean
French National Centre for Scientific Research
75 PUBLICATIONS **1,133** CITATIONS
SEE PROFILE

M. B. Smirnov
Saint Petersburg State University
116 PUBLICATIONS **1,721** CITATIONS
SEE PROFILE

Jose Manuel Gallardo-Amores
Complutense University of Madrid
81 PUBLICATIONS **1,311** CITATIONS
SEE PROFILE

Ulises Amador
University Foundation San Pablo CEU
182 PUBLICATIONS **1,893** CITATIONS
SEE PROFILE

Inorganic Chemistry

Article

pubs.acs.org/IC

Lattice Dynamics of β-V_2O_5: Raman Spectroscopic Insight into the Atomistic Structure of a High-Pressure Vanadium Pentoxide Polymorph

R. Baddour-Hadjean,*[,†] M. B. Smirnov,[‡] K. S. Smirnov,[§] V. Yu Kazimirov,[⊥] J. M. Gallardo-Amores,[¶] U. Amador,[∥] M. E. Arroyo-de Dompablo,[▽] and J. P. Pereira-Ramos[†]

[†]Institut de Chimie et Matériaux Paris-Est, GESMAT, UMR 7182 CNRS et Université Paris-Est Créteil, 2 rue Henri Dunant, 94320 Thiais, France

[‡]Fock Institute of Physics, Petrodvorets, Ul'yanovskaya st., Saint Petersbourg 198904, Russia

[§]Laboratoire de Spectrochimie Infrarouge et Raman, UMR 8516 CNRS et Université Lille1 - Sciences et Technologies, 59655 Villeneuve d'Ascq, France

[⊥]Frank Laboratory of Neutron Physics, Joint Institute for Nuclear Research, Dubna 141980, Russia

[¶]Laboratorio de Altas Presiones, Facultad de Ciencias Químicas, Universidad Complutense, 28040 Madrid, Spain

[∥]Departamento de Química, Universidad San Pablo-CEU, 28668 Boadilla del Monte, Spain

[▽]MALTA Consolider Team, Departamento de Química Inorgánica, Facultad de Ciencias Químicas, Universidad Complutense, 28040 Madrid, Spain

ABSTRACT: We report here the Raman spectrum and lattice dynamics study of a well-crystallized β-V_2O_5 material prepared via a high-temperature/high-pressure (HT/HP) route, using α-V_2O_5 as the precursor. Periodic quantum-chemical density functional theory calculations show good agreement with the experimental results and allow one to assign the observed spectral features to specific vibrational modes in the β-V_2O_5 polymorph. Key structure−spectrum relationships are extracted from comparative analysis of the vibrational states of the β-V_2O_5 and α-V_2O_5 structures, and spectral patterns specific to the basic units of the two V_2O_5 phases are proposed for the first time. Such results open the way for the use of Raman spectroscopy for the structural characterization of vanadium oxide-based host lattices of interest in the field of lithium batteries and help us to greatly understand the atomistic mechanism involved in the α-to-β phase transition of vanadium pentoxide.

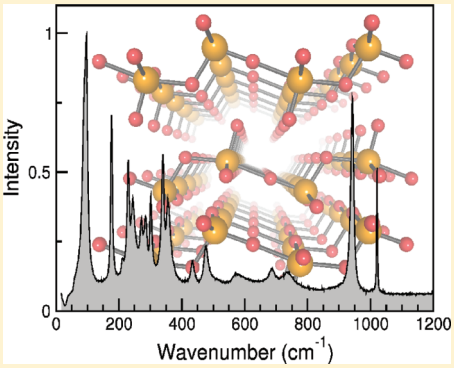

1. INTRODUCTION

Pentavalent vanadium-based frameworks attract much attention because of their outstanding structural flexibility and their chemical and physical properties suitable for catalytic and electrochemical applications.[1−3] The ambient-pressure form of vanadium pentoxide (α-V_2O_5) has a layered structure with orthorhombic symmetry (space group *Pmmn*) consisting of VO_5 square pyramids sharing edges and corners.[4] The structure is well adapted to the reversible incorporation of guest Li^+ ions, and since the 1970s, the α-V_2O_5 polymorph is recognized as an attractive material for applications in electrochromic thin film devices and as a cathode in lithium batteries because of its high energy density and retention capacity upon cycling.[5−11] The valence state of V atoms is known to be extremely sensitive to the chemical environment, and such chemical versatility may lead to a variety of structures containing different building units and exhibiting tunable physical properties. In this regard, high-pressure/high-temperature (HP/HT) synthesis routes are promising ways to obtain novel V_2O_5 polymorphs, particularly for potential electrochemical applications.

The first HP modification of V_2O_5 (prepared at P = 4−6 GPa and T = 650 °C) was reported by Suzuki et al.[12] Later, Volkov et al.[13] reproduced the same HP phase of V_2O_5, named the β phase. Making use of the results of quenching experiments at 600 °C and between 3.5 and 9 GPa, Volkov et al.[13] determined by X-ray diffraction (XRD) measurements that the structure of the β phase is tetragonal. In situ Raman spectroscopic experiments by Grzechnik[14] performed in the pressure range 7−10 GPa and at room temperature (RT) revealed qualitative changes in the Raman spectrum of the V_2O_5 sample, especially in the V−O stretching region. The author concluded that a new phase appeared and coexisted with the α-V_2O_5 starting material; the phase was found to return to the starting orthorhombic material upon pressure release. A few years later, Loa et al.[15] performed similar RT experiments by employing synchrotron radiation for detecting structural changes. The authors observed a pronounced structural disorder under

Received: December 9, 2011
Published: February 23, 2012

   dx.doi.org/10.1021/ic202651b | *Inorg. Chem.* 2012, 51, 3194−3201

elevated pressure and suggested that the correct determination of the new phase necessitates the simultaneous application of HT and HP.

In 2001, two different groups[16,17] published their findings on the V_2O_5 phases investigated at HT/HP, and both reported the existence of the β-V_2O_5 phase with orthorhombic symmetry. Filonenko and Zibrov[16] performed quenching experiments and found the β phase up to 7.5 GPa/900 °C, which returns to the α phase at atmospheric pressure and a temperature of 400 °C. Kusaba et al.[17] showed the presence of the β phase at 6 GPa/500 °C from quenching experiments and at 4.5 GPa/350 °C from in situ experiments. Later, Filonenko et al.[18] reexamined the β phase of V_2O_5 using XRD, neutron diffraction, and high-resolution transmission electron microscopy experiments and found the structure to be monoclinic. The authors established that the β-V_2O_5 structure is built up of infinite chains made of quadruple units of edge-sharing VO_6 octahedra along the b axis. The chains are linked by sharing corners of two octahedra along the c axis, which leads to a V_4O_{10}-layered composition, with the layers parallel to the (100) plane. Weak interactions, similar to those in MoO_3, hold the layers together. Preliminary electrochemical experiments showed that this new monoclinic β-V_2O_5 polymorph behaves as a reversible lithium intercalation compound delivering a specific capacity of 250 mAh/g at a C/3.5 rate.[19] More recently, the V_2O_5 phase diagram was revisited in a wide $P-T$ range (pressures up to 29 GPa and temperatures up to 1500 °C), providing two HP/HT modifications of V_2O_5 (β- and δ-V_2O_5) having well-defined stability ranges in the phase diagram.[20]

Structural distinctions between the α- and β-V_2O_5 polymorphs must become apparent in their vibrational spectra, and the Raman spectroscopy provides a fast, reliable, and nondestructive means of studying these differences. Furthermore, Raman spectroscopy turned out to be a very efficient tool to follow the structural changes under operation conditions for a wide range of transition-metal oxides used as electrode materials for lithium batteries.[26] The Raman spectra of α-V_2O_5 were thoroughly studied both experimentally[21−23] and theoretically.[22,24,25] In addition, Raman studies of the α-V_2O_5/Li system as a pure thin film and as a composite powder electrode were carried out[27−30] and were recently extended to the β-$Na_{0.33}V_2O_5$/Li system.[31]

On the other hand, much less attention was paid to the β-V_2O_5 structure. Up to now, the in situ recorded Raman spectrum at ambient temperatures reported in ref 14 was the only reliable experimental information on vibrational states of β-V_2O_5. However, Raman peaks in this spectrum are markedly large because of strong inhomogeneous broadening due to size/strain effects of pressure gradients in the cells.[15] In the present work, the thermal annealing under pressure is expected to yield a grain coarsening and well-crystallized β-V_2O_5 with a low level of remaining stress, which results in a better quality spectrum.

The Raman spectra measured by Balog et al.[20] on postquench samples retrieved from HP/HT experiments did not show any marked distinction from the spectra of the starting α-V_2O_5 material, although the presence of HP/HT phases was inferred from the XRD experiments. Density functional theory (DFT) calculations confirmed the stability of the β structure[32] and provided a theoretical Raman spectrum[33] of the material that generally agrees with the experimental spectra reported in ref 14. These calculations also ascertained the symmetry assignment of the observed Raman peaks, but the atomistic pattern of the vibrational modes was not presented, and as a consequence, no structure−spectrum relationship was proposed.

This paper reports the results of a combined experimental and computational study of the β-V_2O_5 polymorph. A well-crystallized β-V_2O_5 sample was prepared at HT/HP conditions, and its structure was completely characterized by XRD measurements. A high-quality Raman spectrum of the sample was obtained, and DFT calculations allowed one to assign all of the observed spectral peaks to the vibrational modes of the structure. A comparison of the β-V_2O_5 and α-V_2O_5 vibrational states is provided and leads to the clear identification of spectral features related to the presence of specific structural basic units in the two V_2O_5 polymorphs.

2. EXPERIMENTS AND COMPUTATIONS

2.1. Experimental Part. A commercial (Aldrich) α polymorph of V_2O_5 was subjected to 8 GPa pressure and a temperature of 800 °C for 1 h in a belt-type press. After the pressure and temperature were applied for 1 h, the vessel was quenched to RT while pressure was slowly released. Starting and resulting samples were examined by scanning electron microscopy (SEM) on a JEOL 6400 microscope equipped with an EDAX Inc. energy-dispersive X-ray detector for microanalysis.

The resulting sample was also examined by XRD performed with a Bruker D8 high-resolution powder X-ray diffractometer equipped with an MBraun PSD-50 M position-sensitive detector. Monochromatic Cu $K\alpha_1$ (λ = 1.5406 Å) radiation obtained with a germanium primary monochromator was used. The treatment of the diffraction data was carried out using the *FullProf* program.[34] The structure of the β-V_2O_5 phase reported in ref 18 was employed as a starting model; isotropic thermal parameters and constraints in V−O distances were used to keep the number of the parameter low and to ensure stability of the fitting procedure.

The Raman spectra were measured with a LaBRAM HR 800 (Jobin−Yvon−Horiba) Raman microspectrometer including edge filters and equipped with a back-illuminated charge-coupled device detector (Spex CCD) cooled by the Peltier effect to 200 K. A He:Ne laser (632.8 nm wavelength) was used as the excitation source. The spectra were registered in the backscattering geometry with a spectral resolution of 0.5 cm^{-1}. A 100× objective was used to focus the laser beam to a spot of 1 μm^2 size on the sample surface. To avoid local heating of the sample, the power of the laser beam was adjusted to 0.2−0.5 mW with neutral filters of various optical densities.

2.2. Computational Details. The vibrational states of the two V_2O_5 polymorphs were computed with the *CASTEP* program[35] using density functional perturbation theory (DFPT).[36] The calculations were carried out within the local density approximation (LDA) to DFT and employed Troullier−Martins norm-conserving pseudopotentials.[37] The plane-wave energy cutoff of 35 Ha was used, and the Brillouin zone integration was done over a 2 × 4 × 2 grid of points chosen according to the Monhorst−Pack scheme in the irreducible part of the Brillouin zone. The positions of atoms in the unit cell were optimized with the lattice parameters fixed at their experimental values prior to calculation of the vibrational spectral characteristics. This option was favored over complete geometry optimization because a test calculation of the α-V_2O_5 structure with optimization of both the atomic positions and the lattice parameters, in particular, resulted in a value of the c parameter that was by 14% too small compared to its experimental value. This finding is in a line with that of Zhou and He[25] and is explained by the fact that the LDA fails to correctly describe weak interactions responsible for long V−O contacts (ca. 2.7 Å) between the layers in the structure. A recent computational study by Londero and Schröder[38] showed that dispersion-corrected exchange-correlation functionals need to be used to mimic the interplane spacing in the α polymorph of vanadium pentoxide.

The Raman activity of the vibrational modes was computed within DFPT as described in ref 39. To obtain the Raman scattering

dx.doi.org/10.1021/ic202651b | *Inorg. Chem.* 2012, 51, 3194−3201

intensities, the Raman activities of the vibrational modes were multiplied by Bose–Einstein factors corresponding to the experimental conditions (temperature and wavelength of exciting radiation).

3. RESULTS AND DISCUSSION

3.1. Structure. SEM examination of commercial α-V_2O_5 shows that it consists of large aggregates of particles with a wide distribution in size (up to 50 μm). The HT/HP treatment yields a β-V_2O_5 sample with much smaller aggregates of particles not exceeding 10 μm. We have checked the resulting sample's composition by energy-dispersive spectrometry by analyzing up to 15 particles. The V/O ratio was equal to 2:5 within the experimental error, which confirms the stoichiometric nature of HP-V_2O_5. Furthermore, the sample was verified to be single phase because all of the particles showed the same composition.

The XRD pattern of the quenched sample is shown in Figure 1. All of the diffraction peaks can be assigned to the monoclinic

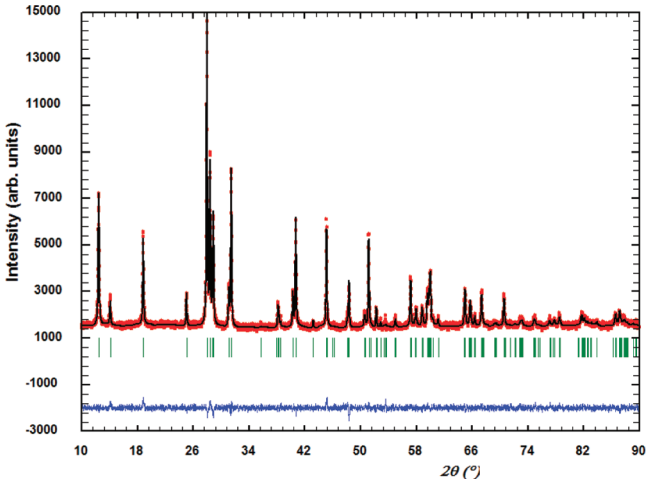

Figure 1. Profile refinement of the XRD pattern corresponding to a sample prepared at a pressure of 8 GPa and a temperature of 1073 K for 1 h in a belt-type press. Red circles: observed pattern. Black line: calculated pattern. Blue line: difference between observed and calculated. The Bragg peaks are indicated by vertical bars.

unit cell previously proposed for the HP form of V_2O_5.[18,32] The final unit cell parameters (space group $P2_1/m$) are a = 7.1016(3) Å, b = 3.5668(1) Å, c = 6.2742(3) Å, and β = 90.121(3)°, and these values are in very good agreement with those determined in previous studies.[18,32]

The microstructural features of the sample were determined by the two-step procedure proposed by Langford.[40] We found an average isotropic crystallite diameter of 374(5) Å and a low level of remaining stress. Thus, the prepared β-V_2O_5 is a well-crystallized and ordered material with low strain effects (for comparison see, for instance, ref 41).

Table 1 compares the fractional coordinates of atoms in the unit cell of the β-V_2O_5 structure obtained in the present study with those given in ref 18 and with the coordinates of atoms optimized in the DFT calculations. The agreement with the literature data is good, and the differences between the two experimental sets of coordinates are explained by the fact that XRD measurements performed in the present work are less precise, especially in locating light O atoms, than the experimental data reported by Filonenko et al.[18] using neutron diffraction. Nevertheless, the results of XRD measurements unambiguously point to the fact that the prepared HP/HT sample is indeed the β phase of vanadium pentoxide. Given the above arguments, the following discussion of the structure β-V_2O_5 makes use of the structural data reported in ref 18.

It is common to consider the structure of V_2O_5 polymorphs as an arrangement of VO_x polyhedra. Such a representation of the α-V_2O_5 structure built of VO_5 polyhedra is shown in Figure 2a. A similar view of the β-V_2O_5 structure in which the V atoms are considered 6-fold-coordinated is given in Figure 2b. In both structures, the VO_x polyhedra share their edges and corners, thus forming layers that are stacked along the z direction and are held together by relatively weak interactions. This structure representation, however, is not fully justified from the crystal chemistry viewpoint because it considers V–O contacts longer than 2 Å as valence bonds.

On the other hand, if considering only contacts with lengths of less than 2 Å as "true" bonds, one can highlight the similarities and differences in the arrangement of structural entities in the crystal lattices of the two V_2O_5 polymorphs. Such a representation of the α- and β-V_2O_5 structures is displayed in Figure 3.

One sees that both structures are built of $[V_2O_5]$ units. Three types of V–O bonds with lengths of less than 2 Å can be identified in the units (Table 2): vanadyl V–O_1 bonds (d_1), V–O_3 bonds (d_2) forming V–O_3–V bridges in the xz planes, and V–O_2 bonds (d_3) forming V–O_2–V bridges oriented along the y direction. The arrangement of the $[V_2O_5]$ units via the d_3 bonds results in $[V_2O_5]_\infty$ chains running in the y direction, and the chains are interconnected by V–O_2 contacts (d_4) longer than 2 Å, which are shown in Figure 3a by dashed lines. As the point symmetry changes from D_{2h} in α-V_2O_5 to C_{2h} in β-V_2O_5, the crystallographic sites of V, O_1, and O_2 atoms split into two nonequivalent groups distinguished by subscripts a and b in Figure 3b,c. In β-V_2O_5, V_a–O_{2b} and V_b–O_{2a} contacts link the chains of two V_2O_5 layers in the z direction (cf. the dashed lines

Table 1. Fractional Coordinates of Atoms in the Unit Cell of the β-V_2O_5 Structure[a]

	expt, ref 18			expt, present work			DFT, present work		
	x/a	y/b	z/c	x/a	y/b	z/c	x/a	y/b	z/c
V_a	0.2773	0.25	0.2557	0.2852	0.25	0.2566	0.2823	0.25	0.2619
V_b	0.0998	0.25	0.8103	0.1035	0.25	0.8070	0.0980	0.25	0.8064
O_{1a}	0.4914	0.25	0.3248	0.4943	0.25	0.3280	0.5004	0.25	0.3245
O_{1b}	0.8241	0.75	0.4374	0.8043	0.75	0.4429	0.8255	0.75	0.4450
O_{2a}	0.1992	0.75	0.2627	0.1910	0.75	0.2521	0.1926	0.75	0.2578
O_{2b}	0.9693	0.25	0.1464	0.9686	0.25	0.1548	0.9708	0.25	0.1409
O_3	0.3012	0.25	0.9576	0.3100	0.25	0.9349	0.3014	0.25	0.9631

[a] R_p = 3.64, R_{wp} = 4.48, R_{exp} = 2.38, χ^2 = 3.55, and Bragg R factor = 3.61.

dx.doi.org/10.1021/ic202651b | Inorg. Chem. 2012, 51, 3194–3201

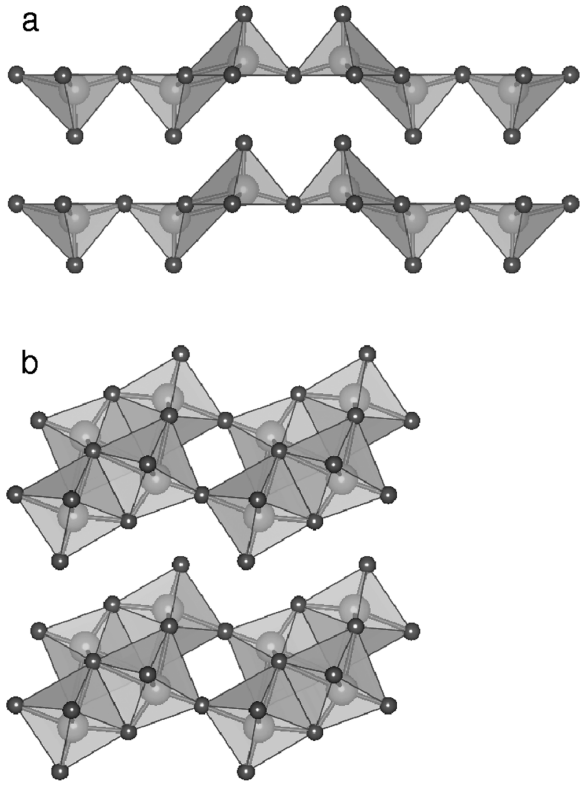

Figure 2. Polyhedral views in the *xz* projection of α-V_2O_5 (a) and β-V_2O_5 (b) structures.

in Figure 3b). Furthermore, half of the vanadyl d_1 bonds in the β-V_2O_5 structure lose their terminal character and transform into highly asymmetric $V_a-O_{1b}-V_b$ bridges. The long V_a-O_{1b} contacts shown in Figure 3b,c by dotted lines connect the chains in the *x* direction. In addition, the $V_a-O_3-V_b$ bridges become asymmetric.

This structural information provides an indispensable basis for the interpretation of the vibrational spectroscopic pattern of the V_2O_5 polymorphs.

3.2. Raman Spectra. Both of the α- and β-V_2O_5 crystal structures contain two formula units per unit cell. According to the group symmetry analysis, 21 Raman-active phonon modes of the α- and β-V_2O_5 polymorphs are distributed over the irreducible symmetry representations as follows:

$$\alpha\text{-}V_2O_5(D_{2h}): \Gamma_{Raman} = 7Ag + 7B_{2g} + 3B_{1g} + 4B_{3g}$$

$$\beta\text{-}V_2O_5(C_{2h}): \Gamma_{Raman} = 14Ag + 7B_g$$

For the α-V_2O_5 structure, vibrational modes involving atomic displacements in the *xz* plane belong to A_g and B_{2g} species, and the modes combine into the A_g representation in the β-V_2O_5 lattice. Similar symmetry distribution is valid for the out-of-plane vibrations with *y* displacements, which belong to B_{1g} and B_{3g} species in α-V_2O_5 and merge into the B_g representation in β-V_2O_5.

The experimental Raman spectrum of the β-V_2O_5 sample is shown in Figure 4a, while Figure 4b presents the Raman spectrum of the α-V_2O_5 material.

The Raman spectrum of β-V_2O_5 exhibits a series of well-resolved peaks, many of which have not been observed previously in the in situ RT/HP experiments[14] and have become evident in the present work. This is related to the microstructure of the sample because thermal annealing under pressure led to a well-crystallized β-V_2O_5 sample with a low level of remaining stress.

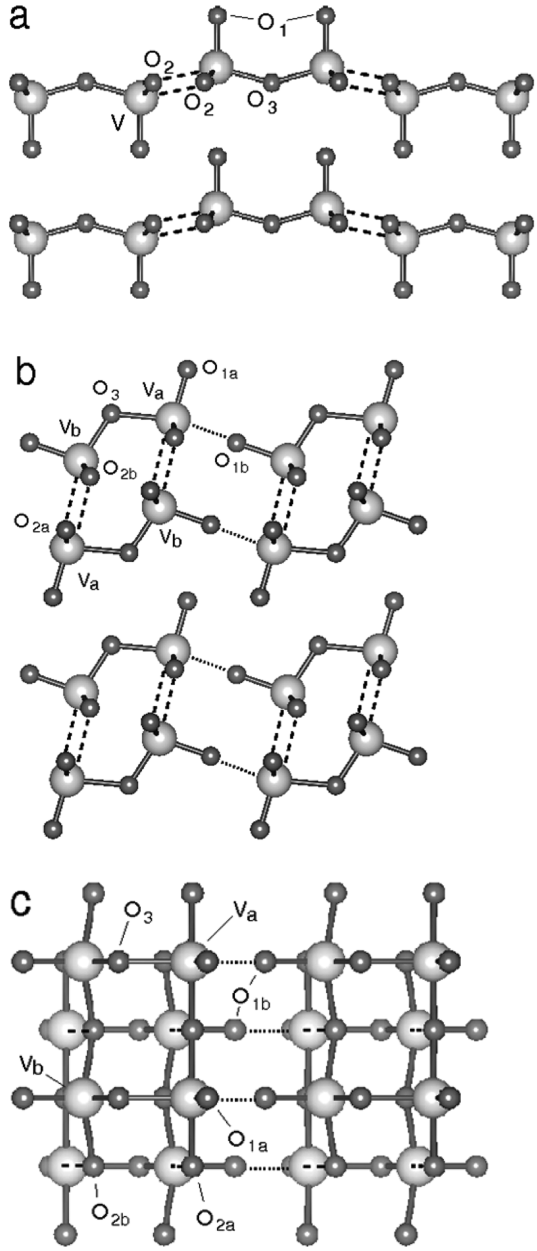

Figure 3. Views of the α-V_2O_5 (a) and β-V_2O_5 (b and c) structures with contacts longer than 2 Å shown as dashed and dotted lines (see the text for details). Images a and b are in the *xz* projection. Image c is in the *xy* projection.

Table 2. Characteristic Interatomic Distances (in Å) in α- and β-V_2O_5 According to the Experimental Data Reported in References 4 and 18

	α-V_2O_5[4]			β-V_2O_5[18]			
d_1	$V-O_1$	1.586	V_a-O_{1a}	1.583	V_b-O_{1b}	1.649	
d_2	$V-O_3$	1.780	V_a-O_3	1.881	V_b-O_3	1.705	
d_3	$V-O_2$	1.878	V_a-O_{2a}	1.871	V_b-O_{2b}	1.872	
d_4	$V-O_2$	2.021	V_a-O_{2b}	2.296	V_b-O_{2a}	2.176	

The following features can be observed:

dx.doi.org/10.1021/ic202651b | *Inorg. Chem.* 2012, 51, 3194–3201

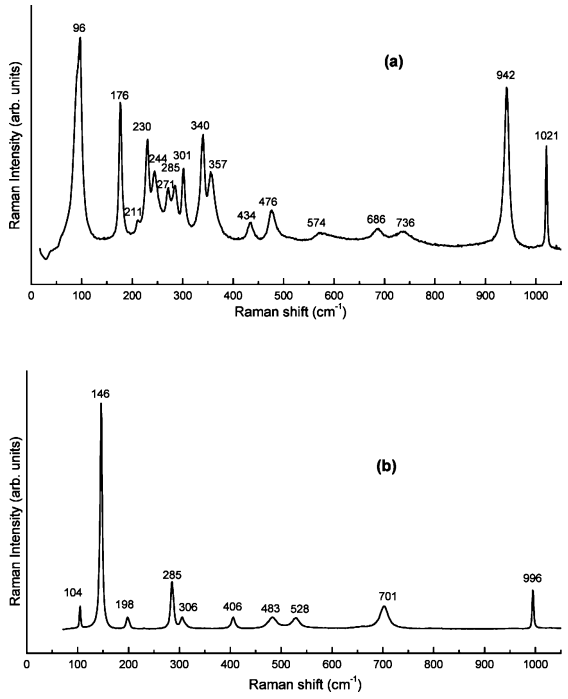

Figure 4. Raman spectra: (a) β-V_2O_5 sample prepared at a pressure of 8 GPa and a temperature of 1073 K for 1 h in a belt-type press; (b) α-V_2O_5 precursor.

(i) Two intense and sharp peaks in the high-frequency region at 942 and 1021 cm^{-1},
(ii) Two large peaks located at 686 and 736 cm^{-1},
(iii) A large peak with a maximum at 574 cm^{-1} and a wide shoulder reaching 620 cm^{-1} from the high-frequency side,
(iv) Two peaks at 434 and 476 cm^{-1}; note that only one peak at ca. 450 cm^{-1} was observed in ref 14.
(v) A number of well-resolved peaks below 400 cm^{-1} with the most intense features at 96, 176, 230, 244, 271, 285, 301, 340, and 357 cm^{-1}. Note that only ill-defined bands with an intense peak at ca. 80 cm^{-1} were observed in this region in ref 14.

The calculated spectrum of β-V_2O_5 is shown in Figure 5, where it is compared with the experimental one. The spectrum

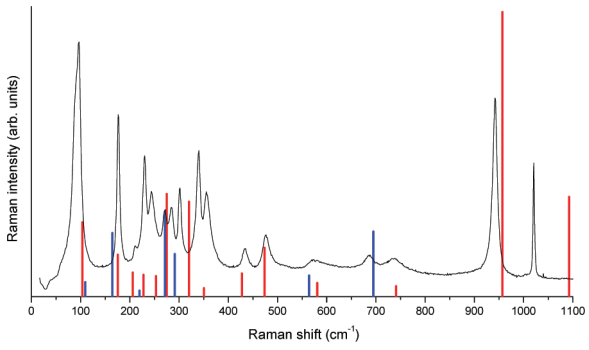

Figure 5. Experimental (black) and computed (color bars) Raman spectra of the β-V_2O_5 sample. Red and blue bars stand for the A_g and B_g vibrational modes, respectively.

well agrees with the theoretical spectrum reported in ref 33.

Table 3 compares the positions of the peaks in the experimental

Table 3. Experimental and Calculated Frequencies and Maximum Atomic Amplitudes of Raman-Active Phonon Modes of the β-V_2O_5 Structure

frequency			max atomic amplitudes[a]		
expt	calcd	symmetry	*x*	*y*	*z*
96	103.5	A_g	L_1–L_2		
96	109.3	B_g		V_a–V_b	
176	164.7	B_g		L_1–L_2	
176	175.4	A_g	O_3		V_a
211	205.6	A_g	O_{1a}		
211	219.8	A_g		O_{1a}	
230	227.6	B_g			L_1–L_2
244	252.9	A_g			O_{1b}
271	271.8	B_g		O_3	
285	274.9	A_g	O_{2a}, O_{2b}		
301	291.3	B_g		O_{1b}	
340	320.4	A_g			O_{2b}
357	350.2	A_g	O_{2a}		O_{1b}
434	427.7	A_g	O_{2b}		
476	473.4	A_g			O_{2a}, O_{2b}
574	581.0	A_g	O_3		
574	564.2	B_g		O_{2a}, O_{2b}	
686	695.2	B_g		O_{2a}, O_{2b}	
736	741.3	A_g			O_3
942	957.0	A_g	O_{1b}		
1021	1092.5	A_g		O_{1a}	

[a] L_1 and L_2 denote translations of neighboring layers.

and computed spectra and proposes the assignment of observed Raman peaks to specific vibrational modes, based on the results of the calculations. One can notice a systematic overestimation of the computed vibrational frequencies in the region above 500 cm^{-1}, which is inherent to the level of theory used. One can also observe that the intensities of some peaks in the low-frequency part of the spectrum are not well reproduced. Nevertheless, a good general correspondence between the spectra allows interpretation of the measured spectral pattern.

Now we turn to assignment of the most prominent spectral features. It is instructive to begin with the α phase of the vanadium pentoxide structure. This consideration will facilitate the subsequent interpretation of the spectral pattern of the more complicated β polymorph. Taking into account the structural data collected in Table 2, one can expect to find four lines in the high-wavenumber region of the Raman spectrum of α-V_2O_5 that correspond to four different bond stretching modes (ν) with frequency relationships

$$\nu(d_4) < \nu(d_3) < \nu(d_2) < \nu(d_1)$$

Furthermore, the O_2 and O_3 atoms are located in symmetric V–O–V bridges and, therefore, the $\nu(d_2)$ and $\nu(d_3)$ modes split into symmetric (s) and antisymmetric (as) components. Only ν_{as}(V–O–V) modes are genuine bond-stretching modes because the ν_s(V–O–V) modes are coupled with the δ(V–O–V) bending modes and thus have markedly lower frequencies. Consequently, one can detail the above relationship as follows:

$$\nu_s(d_2) < \nu_s(d_3) < \nu(d_4) < \nu_{as}(d_3) < \nu_{as}(d_2) < \nu(d_1)$$

The experimental Raman spectrum of α-V_2O_5 (Figure 4b) has four Raman peaks at 996, 701, 528, and 482 cm^{-1}, which were assigned to the $\nu(d_1)$, ν_{as} (d_3), ν (d_4), and $\nu_s(d_2)$ modes, respectively[24,25,28] (Table 4). The missing $\nu_{as}(d_2)$ mode is not

dx.doi.org/10.1021/ic202651b | Inorg. Chem. 2012, 51, 3194–3201

Table 4. Frequencies and Assignments of High-Frequency Raman-Active Phonon Modes of the α-V_2O_5 and β-V_2O_5 Structures

α-V_2O_5		β-V_2O_5				
			max atomic amplitudes			
expt frequency	assignment[24,25,28]	expt frequency	x	y	z	assignment
528	$\nu(d_4)$	476			O_{2a}, O_{2b}	$\nu_s(V_b-O_{2a})$
483	ν_s (d_2)	574	O_3			$\nu(V_a-O_3)$
		574		O_{2a}, O_{2b}		$\nu_{as}(V_b-O_{2b}-V_b)$
701	ν_{as} (d_3)	686		O_{2a}, O_{2b}		$\nu_{as}(V_a-O_{2a}-V_a)$
	ν_{as} (d_2)	736			O_3	$\nu(V_b-O_3)$
996	ν (d_1)	942	O_{1b}			$\nu(V_b-O_{1b})$
		1021			O_{1a}	$\nu(V_a-O_{1a})$

observed because of its low intensity. This feature is related to the structural peculiarity of the α-V_2O_5 structure, where the V−O_3−V bridges are almost linear (cf. Figure 3a) and the $\nu_{as}(d_2)$ mode, being formally Raman-active, has very low Raman activity because of a compensation effect. A theoretical prediction of the frequency of this quasi-silent mode based on a force-field model gave a value of 848 cm^{-1};[22] recent DFT calculations predicted higher values of 936[24] or 1010 cm^{-1}.[25] Regardless the exact value of the $\nu_{as}(d_2)$ wavenumber, one sees that the Raman features in the high-frequency part of the spectrum of the α-V_2O_5 structure can be assigned to the variation of specific structural elements with the use of structural information and common spectroscopic wisdom. It is noteworthy that such an analysis for the low-frequency part of the spectrum is much more difficult because the vibrational modes with frequencies in this region contain important contributions of angle-bending coordinates and involve the dynamics of larger structural entities.

Now we turn to the discussion of the vibrational states of β-V_2O_5. The differences between the α- and β-V_2O_5 structures discussed above are obviously expected to manifest themselves in the vibrational spectra, and given the above structural information, one can await the following changes in the spectrum of the β-V_2O_5 structure compared with that of the α-V_2O_5 polymorph:

(i) Because half of the V−O_1 bonds lose their terminal character, a new peak related to the $\nu(V_b-O_{1b})$ vibration has to appear at a lower frequency.

(ii) Because of the asymmetry of the V−O_3−V bridges in the β phase, the ν_s(V−O_3−V) and ν_{as} (V−O_3−V) modes have to be replaced by the $\nu(V_a-O_3)$ and $\nu(V_b-O_3)$ modes.

(iii) Two B_g modes related to ν_{as}(V−O_2−V) vibrations must split into $\nu_{as}(V_a-O_{2a}-V_a)$ and $\nu_{as}(V_b-O_{2b}-V_b)$ modes.

Analysis of the experimental Raman spectrum of β-V_2O_5 in Figure 4a and of the peak assignments given in Table 4 shows that the observed spectral pattern of the HP phase of vanadium pentoxide indeed follows these expectations:

(i) The spectrum of the β phase has two lines at 942 and 1021 cm^{-1} assigned to the $\nu(V_b-O_{1b})$ and $\nu(V_a-O_{1a})$ modes, respectively, instead of one line at 996 cm^{-1} corresponding to the $\nu(d_1)$ mode in the spectrum of the α phase.

(ii) The $\nu_{as}(d_2)$ and $\nu_s(d_2)$ modes inherent to the vibrations of the bridging O_3 atoms in the α phase become the $\nu(V_b-O_3)$ and $\nu(V_a-O_3)$ modes in the β structure. The former gives rise to the Raman line at 736 cm^{-1}, while the latter contributes to the wide spectral feature centered at 574 cm^{-1}.

(iii) The Raman line at 700 cm^{-1} due to the $\nu_{as}(d_3)$ mode in the α phase splits into two Raman lines in the β phase: the first one, $\nu_{as}(V_a-O_{2a}-V_a)$, is related to the line at 686 cm^{-1}, and the second one, $\nu_{as}(V_b-O_{2b}-V_b)$, contributes to the signal at 574 cm^{-1}.

(iv) The Raman line at 528 cm^{-1} corresponding to the $\nu(d_4)$ mode in the spectrum of α-V_2O_5 undergoes a downward shift to 476 cm^{-1} in the β phase. This line can now be attributed to the $\nu(V_b-O_{2a})$ mode because the V_a-O_{2b} contacts are too long (~2.3 Å) to give rise to a characteristic normal vibration. A signal due to variation of the latter contacts is hidden in a host of low-frequency modes.

The above results allow us to propose fingerprints permitting identification of the α- and β-V_2O_5 polymorphs with the help of Raman spectroscopy:

1 Raman lines around 900 cm^{-1} correspond to the stretching vibrations of vanadyl V═O bonds. A number of such lines indicate the number of nonequivalent vanadyl bonds. It is one for the α phase and two for the β phase.

2 The appearance of two Raman peaks at 736 and 686 cm^{-1} is characteristic of the β-V_2O_5 polymorph. The peak at 736 cm^{-1} points to the presence of the asymmetric V−O_3−V bridge in the β-V_2O_5 structure. In the α phase, the vibrations localized within the symmetric and quasi-linear V−O_3−V bridge manifest themselves as one single $\nu_s(d_2)$ mode located at 482 cm^{-1}, whereas in the β phase, the change of the bridge geometry leads to the appearance of two Raman-active modes at 736 and 574 cm^{-1}.

The second fingerprint peak at 686 cm^{-1} corresponds to a $\nu_{as}(V_a-O_2-V_a)$ mode of B_g symmetry, while the other $\nu_{as}(V_b-O_2-V_b)$ B_g mode contributes to the Raman signal at 574 cm^{-1}. The origin of such a large frequency splitting between the two B_g modes is worth a special comment because similar ν_{as}(V−O_2−V) modes of B_{1g} and B_{3g} symmetry in the α-V_2O_5 structure have almost equal frequencies of 700 cm^{-1}. The 110 cm^{-1} splitting between the B_g modes in the β structure cannot be explained by the difference in the lengths of the V_a-O_{2a} and V_b-O_{2b} bonds, which are equal to 1.871 and 1.872 Å, respectively. Furthermore, both modes involve equal contributions of the $\nu_{as}(V_a-O_{2a}-V_a)$ and $\nu_{as}(V_b-O_{2b}-V_b)$ oscillations.

The splitting can readily be understood by considering the structure of the β-V_2O_5 phase and the displacement of atoms in the two modes. The structure of the vanadium oxide polymorph is characterized by short

dx.doi.org/10.1021/ic202651b | Inorg. Chem. 2012, 51, 3194−3201

$O_{2a}\cdots O_{2b}$ contacts of 2.52 and 2.49 Å in the experimental data and DFT calculations, respectively. Therefore, one might expect a strong influence of O−O interactions on the frequencies of modes with large vibrational amplitudes of the O atoms. Parts a and b of Figure 6

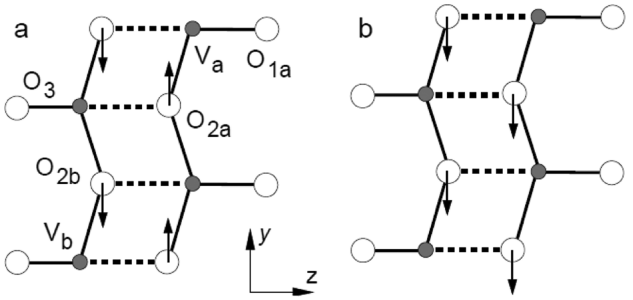

Figure 6. Displacements of O atoms in the two B_g modes with calculated frequencies of 695 cm^{-1} (a) and 564 cm^{-1} (b) of the β-V_2O_5 structure. O and V atoms are shown by white and gray circles, respectively. V−O contacts longer than 2 Å are shown by dashed lines.

show atomic displacements of atoms in the B_g modes experimentally observed at 686 and 574 cm^{-1}, respectively. One sees that the high-frequency mode involves displacements of O_2 atoms in the opposite direction, whereas the atoms move in the same direction in the low-frequency mode. Therefore, the $O_{2a}\cdots O_{2b}$ contacts change their length in the first mode, while they remain unchanged in the second one, and it is just this repulsive O−O interaction that accounts for the 110 cm^{-1} splitting of the vibrational frequencies. It is noteworthy that a similar effect accounts for the features in the Raman spectrum of zircon.[42]

In the case of the α-V_2O_5 structure, the two ν_{as}(V−O_2−V) modes include antiparallel displacements of O_2 atoms similar to those depicted in Figure 6a, and the frequencies of these two modes almost coincide.

3 Finally, the origin of the large spectral band observed in the β phase at around 600 cm^{-1} also merits special consideration. This band has a maximum at 574 cm^{-1} and a wide high-frequency shoulder reaching 620 cm^{-1}. Note that there are no Raman-active modes within this frequency interval in α-V_2O_5. Thus, this spectral feature could also serve as a fingerprint of the β structure. According to our calculations, there are two modes of different symmetry and of almost equal Raman activity within this frequency region: the A_g mode assigned to the $\nu(V_a-O_3)$ vibration and the B_g $\nu_{as}(V_b-O_{2b}-V_b)$ mode with the atomic displacements shown in Figure 6b. The marked difference in the frequencies of these modes in our calculations (A_g, 581 cm^{-1}; B_g, 564 cm^{-1}) can explain the large width of the observed spectral band. Note that the results of ref 33 gave a much smaller frequency difference between these modes (A_g, 611 cm^{-1}; B_g, 613 cm^{-1}).

4. CONCLUSIONS

A well-crystallized sample of the β-V_2O_5 polymorph obtained from the α-V_2O_5 precursor via the HT/HP route was characterized by XRD, SEM, and Raman spectroscopy. A high-quality Raman spectrum is reported with new and well-resolved features, which definitely completes the previous Raman pattern of the β phase of vanadium pentoxide;[14] these experimental data are complemented by periodic quantum-chemical DFT calculations. A good agreement between observed and computed Raman spectra was demonstrated, and the combination of theoretical and experimental techniques provides valuable information, permitting a reliable assignment of all observed spectral features. Comparative analysis of the Raman spectra and phonon states of the β-V_2O_5 phase with those of the parent α-V_2O_5 structure has allowed us to identify for the first time spectral fingerprints specific to structural basic units of the two V_2O_5 polymorphs. The established structure−spectrum correlations are expected to promote the use of Raman spectroscopy for characterization of more complex β-V_2O_5-based structures such as β-$Na_{0.33}V_2O_5$ bronze used as a positive-electrode material in lithium batteries.[31]

AUTHOR INFORMATION

Corresponding Author

*E-mail: baddour@icmpe.cnrs.fr.

Notes

The authors declare no competing financial interest.

ACKNOWLEDGMENTS

M.B.S. gratefully acknowledges the financial support of Université Paris Est Créteil and Université Lille 1. M.E.A.-D. thanks the Spanish Ministry of Science for financial support under Projects MAT2007-62929 and CSD2007-00045. K.S.S. gratefully acknowledges the Centre de Ressources Informatiques of Université Lille 1 for allocation of computational resources.

REFERENCES

(1) Livage, J. *Chem. Mater.* **1991**, *3*, 578.
(2) Chernova, N. A.; Roppolo, M.; Dillon, A. C.; Whittingham, M. S. *J. Mater. Chem.* **2009**, *19*, 2526.
(3) Liu, Z.; Fang, G.; Wang, Y.; Bai, Y.; Yao, K.-L. *J. Appl. Phys. D: Appl. Phys.* **2000**, *33*, 2327.
(4) Enjalbert, R.; Galy, J. *Acta Crystallogr.* **1986**, *C42*, 1467.
(5) Whittingham, M. S. *Chem. Rev.* **2004**, *104*, 4271.
(6) Murphy, D. W.; Christian, P. A.; Disalvo, F. J.; Waszczak, J. V. *Inorg. Chem.* **1979**, *18*, 2800.
(7) Whittingham, M. S. *J. Electrochem. Soc.* **1976**, *126*, 315.
(8) Wiesener, K.; Schneider, W.; Ilic, D.; Steger, E.; Hallmeir, K. H.; Brackmann, E. *J. Power Sources* **1978**, *20*, 157.
(9) Delmas, C.; Cognac-Auradou, H.; Cocciantelli, J. M.; Ménétrier, M.; Doumerc, J. P. *Solid State Ionics* **1994**, *69*, 257.
(10) Bates, J. B.; Gruzalski, G. R.; Dudney, N. J.; Luck, C. F.; Xiaohua, Y. *Solid State Ionics* **1994**, *70/71*, 619.
(11) Cocciantelli, J. M.; Doumerc, J. P.; Pouchard, M.; Broussely, M.; Labat, J. *J. Power Sources* **1991**, *34*, 103.
(12) Suzuki, T.; Saito, S.; Arakawa, W. *J. Non-Cryst. Solids* **1977**, *24*, 355.
(13) Volkov, V. L.; Golovkin, V. G.; Fedyukov, A. S.; Zaynulin, Y. G. *Inorg. Mater.* **1988**, *24*, 1568. Translated from: *Izv. Akad. Nauk USSR Neorg. Mater.* **1988**, *24*, 1836.
(14) Grzechnik, A. *Chem. Mater.* **1998**, *10*, 2505.
(15) Loa, I.; Grzechnik, A.; Schwarz, U.; Syassen, K.; Hanfland, M.; Kremer, R. *J. Alloys Compd.* **2001**, *317/318*, 103.
(16) Filonenko, V. P.; Zibrov, I. P. *Inorg. Mater.* **2001**, *37*, 953.
(17) Kusaba, K.; Ohshima, E.; Syono, Y.; Kikegawa, T. *J. Cryst. Growth* **2001**, *229*, 467.
(18) Filonenko, V. P.; Sundberg, M.; Werner, P.-E.; Zibrov, I. P. *Acta Crystallogr.* **2004**, *B60*, 375.
(19) Arroyo-de Dompablo, M. E.; Gallardo-Amores, J. M.; Amador, U.; Moran, E. *Electrochem. Commun.* **2007**, *9*, 1305.

(20) Balog, P.; Orosel, D.; Cancarevic, Z.; Schon, C.; Jansen, M. *J. Alloys Compd.* **2007**, *429*, 87.
(21) Clauws, P.; Vennik, J. *Phys. Status Solidi B* **1976**, *76*, 707.
(22) Abello, L.; Husson, E.; Repelin, Y.; Lucazeau, G. *Spectrochim. Acta* **1983**, *39*, 641.
(23) Clauws, P.; Broeckx, J.; Vennik, J. *Phys. Status Solidi B* **1985**, *131*, 459.
(24) Brazdova, V.; Ganduglia-Pirovano, M. V.; Sauer, J. *Phys. Rev. B* **2004**, *69*, 165420.
(25) Zhou, B.; He, D. *J. Raman Spectrosc.* **2008**, *39*, 1475.
(26) Baddour-Hadjean, R.; Pereira-Ramos, J. P. *Chem. Rev.* **2010**, *110*, 1278.
(27) Baddour-Hadjean, R.; Rackelboom, E.; Pereira-Ramos, J. P. *Chem. Mater.* **2006**, *18*, 3548.
(28) Baddour-Hadjean, R.; Pereira-Ramos, J. P.; Navone, C.; Smirnov, M. *Chem. Mater.* **2008**, *20*, 1916.
(29) Baddour-Hadjean, R.; Navone, C.; Pereira-Ramos, J. P. *Electrochim. Acta* **2009**, *54*, 6674.
(30) Baddour-Hadjean, R.; Marzouk, A.; Pereira-Ramos, J. P. *J. Raman Spectrosc.* **2011**, DOI: 10.1002/jrs.2984.
(31) Baddour-Hadjean, R.; Bach, S.; Emery, N.; Pereira-Ramos, J. P. *J. Mater. Chem.* **2011**, *21*, 11296.
(32) Gallardo-Amores, J. M.; Biskup, N.; Amador, U.; Persson, K.; Ceder, G.; Moran, E.; Arroyo-de Dompablo, M. E. *Chem. Mater.* **2007**, *19*, 5262.
(33) Zhou, B.; Su, Q.; He, D. *Chin. Phys. B* **2009**, *18*, 4988.
(34) *FullProf*: Rodriguez-Carjaval, J. Satellite Meeting on Powder Diffraction of the XY Congress of the IUCr, Toulouse, France, 1990.
(35) Clark, S. J.; Segall, M. D.; Pickard, C. J.; Hasnip, P. J.; Probert, M. J.; Refson, K.; Payne, M. C. *Z. Kristallogr.* **2005**, *220*, 567.
(36) Refson, K.; Clark, S. J.; Tulip, P. R. *Phys. Rev. B* **2006**, *73*, 155114.
(37) Troullier, N.; Martins, J. L. *Phys. Rev. B* **1991**, *43*, 1993.
(38) Londero, E.; Schröder, E. *Comput. Phys. Commun.* **2011**, *182*, 1805.
(39) Porezag, D.; Pederson, M. R. *Phys. Rev. B* **1996**, *54*, 7830.
(40) Langford, J. I. NIST Special Publication 846. Proceedings of the International Conference on Accuracy in Powder Diffraction II, Gaithersburg, MD, 1992
(41) Fuentes, A. F.; Boulahya, K.; Maczka, M.; Hanuza, J.; Amador, U. *Solid State Sci.* **2005**, *7*, 343.
(42) Lazarev, A. N., Mirgorodsky, A. P., Mazhenov, H. A. In *Vibrations of Oxide Lattices*; Lazarev, A., Ed.; Nauka Publishers: Leningrad, Russia, 1980; pp 72−99.